

# SUPPLEMENTARY MATERIALS

## Control of protein signaling using a computationally designed GTPase/GEF orthogonal pair

Gregory T. Kapp, Sen Liu, Amelie Stein, Derek T. Wong, Attila Reményi, Brian Yeh, James S. Fraser, Jack Taunton, Wendell A. Lim, and Tanja Kortemme

## Supplementary Methods

### Computational specificity redesign

Initial fixed backbone specificity redesign used the computational second site suppressor protocol described previously (1). Flexible backbone specificity redesign employed the sequence tolerance protocol described in (2), using Rosetta revision r33982 and the command lines below.

*Generate an ensemble of structures with the backrub method:*

```
PATH/TO/ROSETTA/backrub.EXECUTABLE -database PATH/TO/ROSETTA_DATABASE  
-s 1kil.pdb -resfile <RESFILE_NAME> -ex1 -ex2 -ex1aro -ex2aro  
-extrachi_cutoff 0 -out:prefix <PREFIX_NAME> -mute core.io.pdb.file_data  
-backrub:ntrials 10000 -score:weights standard_NO_HB_ENV_DEP.wts  
-backrub:minimize_movemap <MOVE_MAP> -nstruct <NUMBER OF MODELS>
```

*Scan for tolerated sequences:*

```
PATH/TO/ROSETTA/sequence_tolerance.EXECUTABLE  
-database PATH/TO/ROSETTA_DATABASE  
-s <BACKRUB_INPUT_STRUCTURE_NAME> -resfile <RESFILE_NAME>  
-ex1 -ex2 -ex1aro -ex2aro -extrachi_cutoff 0 -score:ref_offsets HIS 1.2  
-seq_tol:fitness_master_weights 1 1 1 2  
-ms:generations 30 -ms:pop_size 200 -ms:pop_from_ss 1  
-ms:checkpoint:prefix <NAME> -ms:checkpoint:interval 200  
-ms:checkpoint:gz -score:weights standard_NO_HB_ENV_DEP.wts  
-out:prefix <NAME>
```

### Flexible-backbone design with intensive structural remodeling

Design and remodeling used Rosetta revision r42980, the steps described in SI Results, and Rosetta command lines as below:

### Soft repulsive fixed backbone design

Without ligand:

```
PATH/TO/ROSETTA/fixbb.EXECUTABLE -database PATH/TO/ROSETTA_DATABASE  
-s 1kil.pdb -resfile <RESFILE_NAME> -ex1 -ex2 -ex3 -ex4 -extrachi_cutoff 0  
-score:weights soft_rep_design -out:prefix <PREFIX> -nstruct 30 -overwrite  
-out:pdb_gz
```

With GDP:

```
PATH/TO/ROSETTA/fixbb.EXECUTABLE -database PATH/TO/ROSETTA_DATABASE  
-s <1KII_WITH_GDP> -resfile <RESFILE_NAME> -ex1 -ex2 -ex3 -ex4  
-extrachi_cutoff 0 -score:weights soft_rep_design -out:prefix <PREFIX>  
-nstruct 30 -overwrite -out:pdb_gz -extra_res_fa <PARAMS_FILE>
```

The `PARAMS_FILE` contains instructions for Rosetta on how to handle the ligand, including possible conformation(s). It needs to be specifically generated for each type of ligand. For all simulations reported here, the presence or absence of a GDP ligand in the structure did not lead to significantly different results in terms of backbone RMSD or side chain conformations around the mutated sites (the GDP binding site is distant from the F56R and S1373E mutations, with a distance of 9.9Å between the closest atoms).

### *Backrub ensemble generation*

```
PATH/TO/ROSETTA/backrub.EXECUTABLE -database PATH/TO/ROSETTA_DATABASE  
-s <designed_structure> -in:file:fullatom -ex1 -ex2 -ex3 -ex4  
-extrachi_cutoff 0 -resfile <RESFILE> -out:prefix <PREFIX> -overwrite  
-out:pdb_gz -backrub:ntrials 10000 -nstruct 1 -out:path test  
-mute core.io.pdb.file_data -pivot_residues 330 319 318 212 211 51 324 310  
317 316 315 314 60 234 53 66 67 68 69 80 230 231 171 24 322 20 21 23 320 40  
41 289 323 3 321 5 4 7 6 9 8 328 281 285 327 201 205 204 208 325 329 306 307  
77 76 75 74 73 72 71 70 107 79 78 10 39 38 58 17 16 19 54 57 56 37 36 35 52  
55 333 168 326 292 293
```

`-pivot_residues` determines which residues may be used as pivots by Backrub. This list restricts the pivots to 10Å around the designed residues, using Rosetta's internal residue numbering which is sequential across all chains, starting at 1.

### *Soft repulsive KIC*

```

PATH/TO/ROSETTA/loopmodel.EXECUTABLE -database PATH/TO/ROSETTA_DATABASE
-in:file:fullatom -loops:loop_file <LOOP_FILE> -loops:refine refine_kic
-in:file:native <BACKRUBBED_STRUCTURE>
-loops:input_pdb <BACKRUBBED_STRUCTURE> -score:weights soft_rep_design
-out:prefix <PREFIX> -overwrite -out:pdb_gz -nstruct 1
-out:path <OUT DIR> -vicinity_sampling false -loops:neighbor_dist 6
-ex1 -ex2 -ex3 -ex4 -extrachi_cutoff 0

```

### *Hard repulsive KIC with vicinity sampling*

```

PATH/TO/ROSETTA/loopmodel.EXECUTABLE -database PATH/TO/ROSETTA_DATABASE
-in:file:fullatom -loops:loop_file <LOOP_FILE> -loops:refine refine_kic
-in:file:native <SOFT_KIC_DECOY> -loops:input_pdb <SOFT_KIC_DECOY>
-out:prefix <PREFIX>_ -overwrite -out:pdb_gz -nstruct 1 -out:path <OUT DIR>
-loops:neighbor_dist 6 -ex1 -ex2 -ex3 -ex4 -extrachi_cutoff 0

```

### *Clustering*

```

PATH/TO/ROSETTA/cluster.EXECUTABLE -database PATH/TO/ROSETTA_DATABASE
-l <LIST OF DECOYS> -cluster:radius 0.7 -in:file:fullatom
-ignore_unrecognized_res -native 1kil.pdb -nooutput -exclude_res 1 2 3 4 5 6
7 8 9 10 11 12 13 14 15 16 17 18 19 20 21 22 23 24 25 26 27 28 29 30 31 32 33
34 43 44 45 46 47 48 49 50 51 52 53 54 55 56 57 58 59 60 61 62 63 64 65 66 67
68 69 70 71 72 73 74 75 76 77 78 79 80 81 82 83 84 85 86 87 88 89 90 91 92 93
94 95 96 97 98 99 100 101 102 103 104 105 106 107 108 109 110 111 112 113 114
115 116 117 118 119 120 121 122 123 124 125 126 127 128 129 130 131 132 133
134 135 136 137 138 139 140 141 142 143 144 145 146 147 148 149 150 151 152
153 154 155 156 157 158 159 160 161 162 163 164 165 166 167 168 169 170 171
172 173 174 175 176 177 178 179 180 181 182 183 184 185 186 187 188 189 190
191 192 193 194 195 196 197 198 199 200 201 202 203 204 205 206 207 208 209
210 211 212 213 214 215 216 217 218 219 220 221 222 223 224 225 226 227 228
229 230 231 232 233 234 235 236 237 238 239 240 241 242 243 244 245 246 247
248 249 250 251 252 253 254 255 256 257 258 259 260 261 262 263 264 265 266
267 268 269 270 271 272 273 274 275 276 277 278 279 280 281 282 283 284 285
286 287 288 289 290 291 292 293 294 295 296 297 298 299 300 301 302 303 304
305 306 307 308 309 310 311 312 313 314 324 325 326 327 328 329 330 331 332
333 334 335 336 337 338 339 340 341 342 343 344 345 346 347 348 349 350 351
352 353 354 355 356 357 358 359 360 361 362 363 364 365 366 367 368 369 370
371 372 373 374 375 376 377 378 379 380 381 382 383 384 385 386 387 388 389
390 391 392 393

```

`-exclude_res` specifies the residues to be ignored for RMSD calculation – only those in the flexible loops are considered here. This uses Rosetta's internal residue numbering, which is sequential across all chains, starting at 1.

## Plasmids

All constructs used in this paper are listed in **SI Table S4**. All sequence substitutions were made using the QuikChange mutagenesis system (Stratagene). All sequences were verified by DNA sequencing.

## Protein expression and purification

Proteins were expressed as His6 fusion proteins in the Rosetta2 strain of *E. coli* (EMD Biosciences) using a 3 hour induction with IPTG (Isopropyl  $\beta$ -D-1-thiogalactopyranoside). Cells were lysed by sonication, His6 tagged proteins were bound to Ni-NTA resin (Qiagen) and eluted in 50 mM Na<sub>2</sub>HPO<sub>4</sub>/NaH<sub>2</sub>PO<sub>4</sub>, 300 mM NaCl, 250 mM imidazole, pH 8.0. The His6 tag was cleaved by room temperature incubation with a His6-tagged TEV (Tobacco Etch Virus) protease, followed by removal of the protease and free His6 tags using a second Ni-NTA purification. GTPases were further purified using a SourceQ ion exchange column (Amersham).

GTPase concentrations were determined by the Coomassie Plus system (Pierce). Exchange factor concentrations were determined by absorbance at 280nm using extinction coefficients calculated using the method of Pace *et al.* (3).

## *In vitro* nucleotide exchange assays

For nucleotide dissociation assays, purified GTPases were loaded with mantGDP (methylanthraniloyl-GDP, Molecular Probes) by incubation with a ten-fold molar excess of mantGDP for 30 minutes at room temperature in a buffer of 20mM Tris pH 7.6, 200mM NaCl, 1mM DTT, and 10mM EDTA. Nucleotide loading was quenched by addition of 10-fold molar excess of MgCl<sub>2</sub> above the EDTA concentration and excess nucleotide was removed using NAP-5 columns (GE Healthcare) equilibrated in Exchange Assay Buffer (20 mM Tris, 50 mM NaCl, 10 mM MgCl<sub>2</sub>, 1% glycerol, 1 mM DTT, pH 7.5). Dissociation of mantGDP from GTPases was measured in a SpectraMax Gemini XS (Molecular Devices) fluorescence multi-well plate reader (25°C, excitation: 360 nm, emission: 440 nm). Solutions were pre-equilibrated at 25°C for 10 minutes, and the reaction was initiated by transferring pre-mixed GEF/GDP to mantGDP-bound GTPases. Final concentrations were 1  $\mu$ M mantGDP-bound GTPase, 1  $\mu$ M GEF, 200  $\mu$ M GDP in Exchange Assay Buffer.

For nucleotide association assays, GTPase and GEF were mixed with Exchange Assay Buffer to a final

concentration of 0.5  $\mu$ M for GTPase and varying concentrations of GEF. The solutions were equilibrated for 10 minutes before the addition of mantGDP to a final concentration of 400 nM to start the reaction. Reaction progress was monitored by fluorescence as above. Rates were determined by linear fits to the initial rates of exchange (4). The fold catalysis was determined by dividing the catalyzed rate by the uncatalyzed rate (for the GTPase alone without GEF).

### **Circular dichroism (CD) spectroscopy**

CD data were collected on each protein (Cdc42 and ITSN, WT and variants) at concentrations close to 10 $\mu$ M on an Aviv CD spectrophotometer. CD data collection was done in a buffer of 10 mM sodium phosphate, pH 7.0, and 100 mM NaCl, in a 0.2 cm cuvette. Samples were cooled to 4°C and then heated to 90°C and the ellipticity at 222 nm recorded at 3°C increments. Ellipticity was converted to mean residue ellipticity (MRE).

### **Surface plasmon resonance**

All experiments were performed on a Biacore T100 instrument using a running buffer of HBS-P (0.01 M HEPES, 0.15 M NaCl, pH 7.4, 0.005% v/v Tween 20) with the addition of 50  $\mu$ M EDTA. Roughly 600 response units (RU) of GEF were immobilized on a CM5 sensor chip (Biacore) using the amine coupling kit. Injections at a number of concentrations (0, 10, 30, 50, 75, 100, 150, 200, 250, 350, 500, 1000 nM) of analyte (Cdc42<sup>WT</sup> or *ortho*Cdc42) were used to determine the equilibrium binding affinities. Injections at concentrations above 1000nM showed evidence of non-specific binding events and were not used in the affinity determination. All injections were performed at 25 °C at a flow rate of 25  $\mu$ L/min with a 180 second association phase, a 240 second dissociation phase, a 30 second regeneration in HBS-P + 10 mM MgCl<sub>2</sub> + 1 mM GTP, and a final regeneration of 20 seconds of HBS-P + 5 mM EDTA. Equilibrium data were analyzed using Biacore Evaluation software (version 1.1.1) and the Rmax for each injection series was fit using the Steady State Affinity Fit with the offset at zero. The affinity values reported are the average of three concentration series.

### **Crystallography**

The *ortho*Cdc42 (F56R) and *ortho*ITSN DH/PH (S1373E) proteins were purified using the NiNTA resin and the His6 tags were cleaved and removed as described above. Each protein was then further purified by gel filtration over a Sephadryl S100HR column (Amersham) in a buffer of 50 mM sodium phosphate (pH 7.4) and 150 mM NaCl. Purified proteins were concentrated in a buffer of 20 mM Tris pH 7.5, 150 mM NaCl, 2 mM EDTA, and 1 mM DTT and then combined in a 1:1 molar ratio to a final concentration of 10mg/mL.

X-ray diffraction data were collected on beam 8.3.1 at the Advanced Light Source at Lawrence Berkeley National Laboratory. A single data set was collected from a crystal diffracting to 2.65 Å and processed in space group P21 with HKL2000 (5), phased by molecular replacement using AMORE (6) with 1KI1 as a search model. Rebuilding was performed manually with Coot (7) with iterative refinement using phenix.refine (8) using non-crystallographic symmetry between the two copies of the *ortho*ITSN/*ortho*Cdc42 complex present in the asymmetric unit.

### **WASP fluorescence titration**

WASP fluorescence titrations were performed as described previously (9). The W13 fragment of WASP(9) (residues 201-321) was cloned into a His6 expression vector, expressed and purified as described in the main Methods for GTPase and GEF proteins, and the His6 tag was cleaved by treatment with TEV protease. The W13 concentration was determined using an extinction coefficient ( $E_{280}$ ) of 8250 M<sup>-1</sup> cm<sup>-1</sup> (9). Purified Cdc42<sup>WT</sup> and *ortho*Cdc42 were preloaded with mantGMPPNP (Molecular Probes) as described in the main Methods for mantGDP. Proteins were diluted in 40 mM HEPES-NaOH pH 7.4, 100 mM NaCl. A 1 cm<sup>2</sup> cuvette was filled with a 200 nM solution of Cdc42•mantGMPPNP and maintained at 25 °C. The decrease in Cdc42•mantGMPPNP fluorescence with W13 addition was monitored using a Photon Technologies International (Birmingham, NJ) fluorimeter with excitation and emission set to 360 nm and 440 nm, respectively. Titrations were performed by manual injections of W13 solution using a Hamilton syringe allowing for 1 minute of mixing before averaging fluorescence emission for 2 seconds. Raw data were corrected for Cdc42 concentration and then fit as described (9).

### **GAP assay**

GTP hydrolysis by Cdc42 was tested using the EnzChek Phosphate Assay Kit (Invitrogen) and the assay protocol of Zhang *et al.* (10). Briefly, 8 µM soluble Cdc42 was combined with 5 mM MgCl<sub>2</sub>, 0.2 mM GTP (Roche), 0.2 mM 2-amino-6-mercaptopurine riboside (MESG), and 0.5 units of purine nucleoside phosphorylase (PNP) in 50 mM Hepes pH 7.5, 0.1 mM EDTA. Inorganic phosphate released by Cdc42 coupled to the MESG by the PNP to generate a product with an absorbance at 360 nm. Absorbance readings were made using a SpectraMax Plus (Molecular Devices) reader. The addition of 1-4 nM of p50RhoGAP produced an increase in the rate of GTP hydrolysis (observed as a more rapid increase in absorbance).

### **N-WASP translocation to beads**

Full-length Cdc42<sup>WT</sup> and *ortho*Cdc42, including the C-terminal CAAX motif, were expressed as His6-tagged proteins in SF9 cells. SF9 lysates were combined with *E. coli* lysates expressing GST-tagged

bovine RhoGDI protein. The RhoGDI•Cdc42 complexes were then purified using a Ni-NTA column followed by a GST-agarose column (Amersham). For the assay, glass beads (2.3  $\mu$ m diameter; Bangs Laboratories) were coated with a lipid mixture of 75% phosphatidylcholine, 20% phosphotidylserine, and 5% PIP2 and incubated with 50  $\mu$ M GTP $\gamma$ S, 1 mM MgCl<sub>2</sub>, 1 mM DTT, and the indicated full-length Cdc42 protein (complexed with RhoGDI) and ITSN protein for 20 minutes. The final concentrations were 1  $\mu$ M Cdc42•RhoGDI complex, 1  $\mu$ M ITSN<sup>WT</sup> or 2.5  $\mu$ M *ortho*ITSN. Fluorescent N-WASP (dEVH1 construct, residues 137-502; Alexa 594 labeled) was then added to a final concentration of 1  $\mu$ M and allowed to localize for an additional 20 minutes. The beads were fixed and imaged on an Olympus IX70 microscope at 60x magnification. The fluorescence intensity of individual beads was measured by determining the total integrated fluorescence of a 2.5  $\mu$ m diameter circle enclosing the bead and subtracting the fluorescence of the same circle enclosing only background fluorescence (no beads). For each condition at least 20 individual beads were measured.

### Nucleofection

The Cell Line 96-well Kit SE from Lonza Cologne AG was used to transfect the plasmids (all constructs are as listed in **Table S4**) into NIH 3T3 cells. The cells were cultured in DMEM (Dulbecco's Modified Eagle Medium) containing 10% bovine calf serum (BCS) to 70-80% confluence, trypsinized, spun and resuspended in the manufacturer's SE solution (20  $\mu$ L for  $6 \times 10^5$  cells). Then 20  $\mu$ L of cells were mixed with 1  $\mu$ g total of pre-mixed indicated plasmids in 2  $\mu$ L total volume, and transferred to a 96-well Nucleocuvette Plate well. The nucleofection was performed in the 96-well Shuttle system with the standard 96-CA-137 program. After incubating at room temperature for 10 min, 80  $\mu$ L of DMEM (10% BCS) were added to each well.

### G-LISA assay

The Cdc42 G-LISA Kit (Cytoskeleton) was used to detect active GTP-bound Cdc42 in NIH 3T3 cells. 12-well culture plates were prepared by adding 1 mL of DMEM containing 10% BCS. After the nucleofection step, for each transfected sample, the cells were transferred to two prepared wells on the 12-well culture plates with 50  $\mu$ L cells per well. After 8 h of culture followed by 7 h of starvation, for each transfected sample, Rapamycin in DMEM without serum was added to a final concentration of 20  $\mu$ M to the cells in one well, and the other well served as the control by adding the same volume of DMSO as Rapamycin in DMEM without serum. Then, the medium was aspirated off at the indicated time points, and G-LISA Lysis Buffer was added to lyse the cells. The lysates were flash frozen in liquid nitrogen and stored at -70°C. The G-LISA assay was performed as specified as in the manufacturer's manual, after the lysates were diluted with G-LISA Lysis Buffer containing protease inhibitors to 0.7mg/mL total protein.

### **ELISA assay**

To measure the total Cdc42 loaded for G-LISA assay, the wells of ELISA plates were first coated with Chicken Polyclonal IgY Antibody to Cdc42 (AbCam). Then the cell lysates (same lysates as above) were added into the wells for Cdc42 binding, followed by adding an HRP-conjugated anti-Cdc42 monoclonal antibody (Santa Cruz Biotechnology) to Cdc42. TMB (3,3',5,5'-tetramethylbenzidine) substrate solution was used for detection, and the absorbance at 450nm was measured after the addition of 1 M H<sub>3</sub>PO<sub>4</sub> to stop the reaction.

### **Live cell fluorescence microscopy**

After the nucleofection step, NIH 3T3 cells were cultured in 8-well Lab-Tek II Chambered Coverglass wells. After the same serum starvation process as described above, pictures were taken on a Nikon Eclipse Ti Microscope with a 60X or 100X objective at 37 °C. Rapamycin was added to a final concentration of 20 μM as above.

### **xCELLigence assay**

The xCELLigence System (Roche Applied Science) can be used to monitor cell morphological changes in real time without the incorporation of labels. The electrode impedance, which is defined as cell index (CI) values, is correlated with the change of cell morphology (11). The xCELLigence system E-plate wells were coated with 40 μg/mL Fibronectin (Sigma-Aldrich) for 1 h at 37 °C. After washing with phosphate-buffered saline (PBS: 137 mM NaCl, 2.7 mM KCl, 10 mM Na<sub>2</sub>HPO<sub>4</sub>, 2 mM KH<sub>2</sub>PO<sub>4</sub>, pH 7.4), the wells were blocked with 0.5% bovine serum albumin (BSA) solution in PBS for 20 min at 37 °C. 100 μL DMEM containing 10% BCS were added to each well after washing with PBS, and then the E-plates were equilibrated in an incubator (37 °C, 5% CO<sub>2</sub>). After the NIH 3T3 cells were transfected with indicated plasmids as described in the main Methods, 15 μL of transfected cells were transferred to each prepared E-plate well. The E-plates were then placed on the xCELLigence machine for real-time recording every 3 min. After eight hours, the medium in each well was changed to 100 μL of DMEM without serum for starvation. After 7 h of serum starvation, the data recording frequency was changed to 15 seconds and Rapamycin (Sigma-Aldrich) in DMEM without serum was added to each well to the final concentration of 20 μM.

## Supplementary Results

### Other designed ITSN variants using fixed and flexible backbone design

**Table S1** lists other predicted ITSN variants tested both in the context of Cdc42<sup>WT</sup> and *ortho*Cdc42. In addition to the ITSN S1373E variant, two other ITSN mutations were tolerated in the designed interface; the mutations were either predicted in sequences designed using flexible backbone simulations (M1369L) or observed in several ITSN homologs and predicted to be favorable (L1376I). In contrast, the ITSN Q1380E mutation, which was the most frequently observed mutation in fixed backbone design simulations (**Fig. 1D**), was not active towards *ortho*Cdc42 (**Fig. S2**) when tested in combination with S1373E (which was present simultaneously, although much less frequently, in fixed backbone simulations). These results illustrate the difficulty in correctly predicting the precise details of polar interactions in protein interfaces, in particular when using fixed backbone approaches.

The L1376W substitution in ITSN, which was predicted in flexible backbone simulations to be favorable for the interaction with Cdc42<sup>WT</sup> (**Fig. S1C**), and also to be tolerated by *ortho*Cdc42 (**Fig. 1D**) was not active in either context (**Fig. S2**), possibly because of steric incompatibilities that result from overpacking.

### Interactions with other GTPases and GTPase binding partners

The DH/PH domains of the exchange factor Dbs catalyze exchange in Cdc42<sup>WT</sup> but not in *ortho*Cdc42 (**SI Table S3**). One exchange factor, the DH domain of PREX1, is able to catalyze nucleotide exchange in both Cdc42<sup>WT</sup> and *ortho*Cdc42, whereas others, such as the DH/PH domains of the exchange factors Tiam1 and Trio (the N-terminal DH/PH) do not catalyze exchange in either Cdc42<sup>WT</sup> or *ortho*Cdc42 (**SI Table S3**). These results suggest that our design was successful in specifically perturbing the interaction with ITSN and the highly similar GEF Dbs.

Because ITSN is an exchange factor specific for Cdc42, ITSN does not catalyze nucleotide exchange in the Rac1 or RhoA GTPases, and *ortho*ITSN does not change this intrinsic specificity (it does not catalyze exchange in either Rac1 or RhoA, **SI Table S3**).

### Transferability of the designed mutations to a related GTPase/GEF interaction

Given the unique nature of the engineered complementary F56R/S1373E substitutions in the Cdc24/ITSN interface, we asked whether they could be transferred into another GTPase-GEF interface to make that interaction orthogonal with respect to the original wild-type binding partners and possibly other related GTPases and GEFs. However, simply porting the R-E pair to the structurally equivalent positions in the

Rac1-Tiam1 interface was not successful in compensating for the detrimental effect of each of the mutations alone (**SI Fig. S9**). This result is not surprising, given the intricate nature of coupled residue-residue interactions in proteins and protein-protein interfaces. Interestingly, repeating our flexible backbone design prediction protocol as illustrated in **Figure 1D** on the crystal structure of the Rac1-Tiam1 complex corroborates this result and does not show enrichment for negatively charged amino acids at the Tiam1 position equivalent to 1373 in ITSN (**SI Fig. S10**).

### Structural Analysis

The overall backbone C $\alpha$  RMSD values between the *ortho*Cdc42/*ortho*ITSN and the Cdc42<sup>WT</sup>/ITSN<sup>WT</sup> complex structure (PDB ID: 1KI1) are 0.58 Å and 0.47 Å for the Cdc42 molecules and the ITSN DH domains, respectively (**SI Fig. S5A**). However, there are regions with larger deviations in the backbone, in particular the loop around Y40 in Cdc42, which rearranges to accommodate side chain movements triggered by the mutations, as discussed in the main manuscript (**Fig. 3**). This region has a C $\alpha$  RMSD of 1.998 Å in the 36-43 loop. While the DH domain of ITSN forms the interface with Cdc42, the PH domain of *ortho*ITSN (which is spatially distant from the interface and thus the site of mutation) has poor density in our complex structure for a significant portion of the mainchain, and the orientation of the ITSN PH domain relative to the Cdc42 molecule differs in the two crystal structures, indicating possible domain-domain flexibility in solution. The different orientation in our structure results in a change to the crystal lattice.

The designed complex structure has defined electron density in the active site of *ortho*Cdc42 (**SI Fig. S5C**). In the course of refining the *ortho*Cdc42/*ortho*ITSN structure, this density persisted through simulated annealing omit and kicked map calculations. Based on the shape of the electron density, we modeled a GDP molecule bound in the active site of the *ortho*Cdc42/*ortho*ITSN, bound in the same orientation as Cdc42<sup>WT</sup> without any associated exchange factor (PDB ID: 1AN0, **SI Fig. S5D**). This electron density was surprising because the side chain of A59 is in essentially the same conformation as A59 in the Cdc42<sup>WT</sup>/ITSN<sup>WT</sup> structure (PDB ID: 1KI1, **SI Fig. S5E**). The position of A59 triggered by GEF binding is assumed to displace the Mg<sup>2+</sup> ion necessary for binding a GDP molecule. In contrast, the conformation observed in the Cdc42<sup>WT</sup> structure (PDB ID: 1AN0, **SI Fig. S5D**) is compatible with Mg<sup>2+</sup>-binding. The active site residues of Cdc42 bound to ITSN would not clash directly with GDP. Rather, the direct clash of A59 with the Mg<sup>2+</sup> atom, which likely disfavors GDP binding, leads to higher GDP mobility and an increased probability of dissociation. The B-factors for the GDP molecule were higher than the surrounding protein atoms (~80 vs 54 for the protein). Since the resolution is not sufficient to refine occupancies or to observe any correlated structural changes in the protein, the simplest explanation

is that the density represents a relatively disordered GDP molecule bound in the active site of *ortho*Cdc42. In the Cdc42<sup>WT</sup>/ITSN<sup>WT</sup> complex structure, an electron rich sulfate molecule is modeled in a position that overlaps with the placement of the beta-phosphate of the putative GDP (**SI Fig. S5E**). However, structure factors for this complex were not deposited, so electron maps cannot be calculated to determine if the density extends beyond the sulfate position. Currently we cannot distinguish whether the GDP molecule present in the *ortho*Cdc42/*ortho*ITSN is due to the engineered mutations, an intermediate conformation in nucleotide exchange, or would also be observed in the wild-type complex.

### Flexible-backbone structure remodeling

To test whether the observed conformational changes in the *ortho*Cdc42/*ortho*ITSN interface could be computationally recapitulated, we implemented an initial version of a flexible backbone design and remodeling protocol intended to predict significant structural changes in response to designed mutations (**Figure S6A**). This protocol uses two general concepts: The first is switching between steps that diversify backbone conformations and steps that focus sampling in certain regions of conformational space. This idea has been used successfully in protein structure refinement (12). Different backbone remodeling algorithms employing “backrub” (13) and “kinematic closure” (KIC) (14) moves allow us to diversify the conformations of the protein as well as to determine regions surrounding the designed positions that are particularly flexible and thus more likely to change upon mutation (12). The second concept is interleaving soft and hard repulsive forces, which enables us to model conformational changes that initially appear unfavorable, but may be accommodated by subsequent refinement steps using intensified sampling in defined regions. Successful application of this concept has recently been reported in protein structure refinement (15).

Modeling of the *ortho*Cdc42/*ortho*ITSN complex used the general protocol outlined in **Figure S6A** with the following steps and simulation details:

1. Design, soft potential: We introduced the two designed mutations, F56R and S1373E, into the template structure (PDB ID: 1KI1), keeping the backbone fixed and repacking the side chains in a 10 Å radius around the mutations. This step used the Rosetta all atom energy function with soft repulsive forces, which allow slightly unfavorable conformations of the side chains to still be accepted.
2. Initial backbone diversification, hard potential: Backbone diversification of the initial design model employed backrub moves (13) in a 10 Å radius around the mutations using the Rosetta all atom energy function with hard repulsive forces. This step generated an ensemble of 1200 structures with slight variations in the backbone that may accommodate the designed residues, while reducing possible steric clashes from the soft repulsive design step. The overall structural variation in this

ensemble is low, however, and none of the structures is very close in backbone RMSD to the *ortho*Cdc42/*ortho*ITSN crystal structure (**Figure S6B**).

3. Aggressive backbone diversification, soft potential: To generate larger diversity, the next diversification step employed kinematic closure (KIC) refinement moves with soft repulsive forces. Sampling was focused on two loop regions (36-44 in Cdc42 and 1365-1370 in ITSN) in a 10 Å radius of the mutated positions. To determine these focus regions in an unbiased fashion, we selected regions that showed the largest conformational variability in initial backbone diversification simulations of the template structure (PDB ID: 1KI1, **Figure S6C**). This selection criterion follows the rationale described in (12) that regions with the largest simulated diversity in initial models are often the regions that show the largest deviation from the native structure. **Figure S6D** shows that many of the models resulting from the intense KIC backbone diversification step moved closer to the *ortho*Cdc42/*ortho*ITSN crystal structure.
4. Intensification and refinement, hard potential. To intensify sampling around low-energy conformations identified in the previous step, the final simulation step employed KIC refinement moves in the same variable regions as in step (3) with hard repulsive forces using vicinity sampling, which restricts the sampled backbone angles to those similar to the input model. 600 input models were selected from the 10,000 decoys from step (3), using the following criteria: The 10,000 decoys were first binned by RMSD to the flexible regions in the template (so only information of the template structure was used, as in a general application the structure of the target, the designed complex, will not be known). Then, to represent the diversity of conformations sampled in step (3), we selected representative decoys from each bin such that the number of selected decoys scales logarithmically with the total number of structures in that bin, always choosing the lowest-energy decoys (**Figure S6E**). The intensification and refinement step adapts both backbone and side chains to remove clashes or unfavorable conformations that may have arisen in the preceding soft remodeling step. Application of KIC moves as well as repacking of the surrounding side chains and minimization of backbone and side chain torsion degrees of freedom resulted in considerably lower Rosetta energies (**Figure S6F**, compare with **Figure S6D**).
5. Clustering. **Figure S6F** shows that, while conformations very close (< 1 Å backbone RMSD) to the crystal structure of the designed complex are sampled, they cannot be distinguished by energy from other sampled conformations. However, clustering the 2400 models resulting from step (4) by the C $\alpha$  RMSD of the two flexible regions (between all pairs of models, again not considering information from the solved structure) clearly identifies a conformation close to the designed crystal structure for two of the six dominant clusters (**Figures S6G, Fig. 3** in the main manuscript).

### Cell-based assays

In all cell-based assays, we transiently transfected NIH 3T3 cells with combinations of plasmids encoding FKBP-ITSN, Cdc42 and Lyn-FRB, as indicated (**Fig. 5** in the main manuscript). ITSN and Cdc42 constructs were additionally tagged with fluorescent proteins (**SI Table S4**) to assess expression levels and localization. Prenylated Cdc42 is expected to be localized to the plasma membrane or bound to Rho-GDI. The ITSN-FKBP construct remained predominantly cytoplasmic until the addition of the small molecule Rapamycin.

We also measured induced morphological changes using the label-free xCELLigence system (Roche). Cells transiently transfected with indicated plasmids adhere to E-plate wells covered with gold electrodes. Morphological changes of cells (due to the activation of Cdc42) cause a change of the electrode impedance, which is detected in real time and displayed as changes of cell index (CI) values. Although small, we observed reproducible differences for the different transfected cognate and non-cognate Cdc42/ITSN pairs that were overall consistent with the cell-based results on Cdc42 activation and morphological changes discussed in the main manuscript. As shown in **SI Figure S8B**, we first observed similar spikes for all samples in the first 30 seconds after the addition of Rapamycin; these spikes were likely dominated by the change of environment since they were still seen when only medium (including DMSO) without rapamycin was added. The most noticeable differences are between 30 seconds and 90 seconds after the addition of Rapamycin. During that time, the signals of presumed negative samples (the non-cognate  $\text{Cdc42}^{\text{WT}}/\text{orthoITSN}$  pair and transfections without the recruiter domain Lyn-FRB) decreased noticeably. In contrast, the signal for the designed cognate pair  $\text{orthoCdc42}/\text{orthoITSN}$  (with Lyn-FRB) stays high for about 90 seconds, which was also true for the positive control,  $\text{Cdc42}^{\text{WT}}/\text{ITSN}^{\text{WT}}$  (with Lyn-FRB). At longer times, the signal for the designed pair appears to decrease faster than that of the wild-type cognate pair. Decreasing signals at longer times could be caused by retraction of cells as seen in **SI Figure S8C**, although we observe similar retraction also for the wild-type pair. As discussed in the main manuscript, we observe a positive signal for the other non-cognate pair  $\text{orthoCdc42}/\text{ITSN}^{\text{WT}}$ , likely due to the presence of endogenous  $\text{Cdc42}^{\text{WT}}$ . Taken together, the XCELLigence results indicate that: First, transfection of  $\text{Cdc42}^{\text{WT}}$  has the most significant signal changes when  $\text{ITSN}^{\text{WT}}$  was recruited to the membrane, but not with  $\text{orthoITSN}$ ; and second, recruitment of  $\text{orthoITSN}$  induced more significant signal changes when  $\text{orthoCdc42}$  was present than with  $\text{Cdc42}^{\text{WT}}$ .

## Supplementary Figures

### Figure S1: Additional modeling and design simulations.

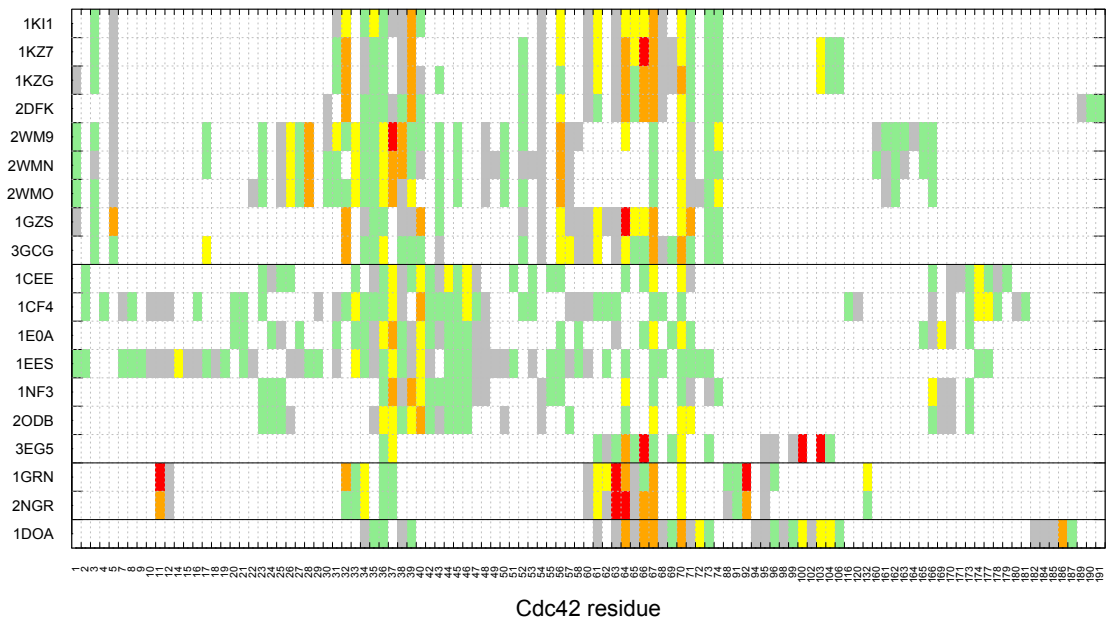
**(A)** Computational alanine scanning. Shown are the estimated effects on binding energy of replacing each residue in Cdc42 with alanine in the context of 19 co-complex structures of Cdc42 with partner proteins. Representation is as shown in Figure 1C in the main manuscript, but results are shown for all Cdc42 residues (instead of just Cdc42 residues in the interface with ITSN taken from PDB ID 1KI1). White blocks mean missing or non-interface residues.

**(B)** Application of fixed backbone computational second site suppressor design, as described in (1). F56 of Cdc42 was computationally mutated to all amino acids (except cysteine) and the effect on complex destabilization was computed (red bars,  $\Delta\text{score}$  (destabilization) = score (complex Cdc42(mutant)/ITSN<sup>WT</sup>) – score (complex Cdc42<sup>WT</sup>/ITSN<sup>WT</sup>)). In a second simulation, the residues on ITSN in the vicinity of position 56 on Cdc42 are designed in the presence of the single mutation on Cdc42 to compensate for the change, and again the effect on the complex binding energy was estimated (blue bars,  $\Delta\text{score}$  (compensation) = score (complex Cdc42(mutant)/ITSN(designed)) – score (complex Cdc42(mutant)/ITSN<sup>WT</sup>)). Amino acids at position 56 (x axis) are ordered by the  $\Delta\Delta\text{score}$  (black bars) =  $\Delta\text{score}$  (compensation) -  $\Delta\text{score}$  (destabilization).

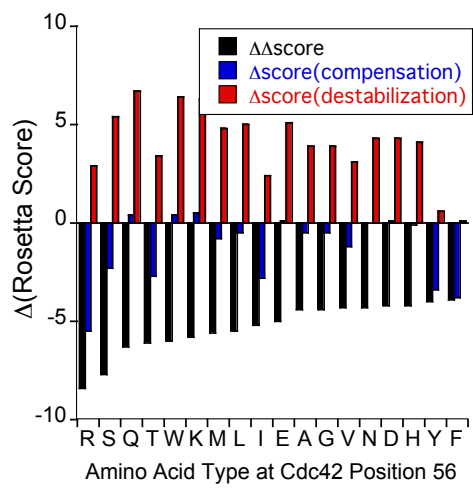
**(C)** Flexible backbone computational design predictions (**Methods**) for the four residues in ITSN neighboring position 56 of Cdc42<sup>WT</sup>. Simulations are exactly as shown in Figure 1D in the main manuscript, except that the Cdc42 does not contain a modeled F56R mutation. Figure was prepared with WebLogo.

**Figure S1**

**A**



**B**



**C**

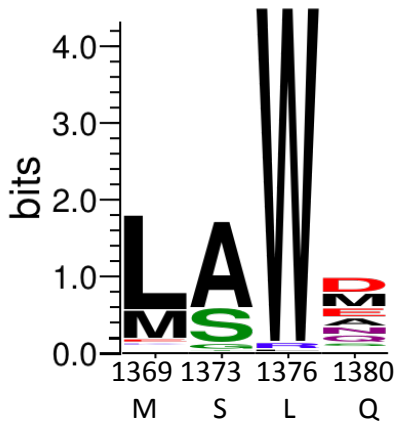


**Figure S2: Nucleotide exchange for additional designed ITSN variants.**

Catalysis of nucleotide exchange in  $\text{Cdc42}^{\text{WT}}$  (left) and  $\text{orthoCdc42}$  (right) by different ITSN variants. ITSN variants were predicted from flexible backbone design simulations (**Figure 1D** in the main manuscript). Shown is the fold increase of initial rates of mant-GDP association to  $\text{Cdc42}$  at varying GEF concentrations over  $\text{Cdc42}$  alone. Data represent averages and standard deviations from three experiments. Mutation(s) in ITSN:  $\text{orthoITSN}$  represents S1373E,  $^{**\text{W}^*}$  L1376W,  $^*\text{E}^*\text{E}$  S1373E-Q1380E.

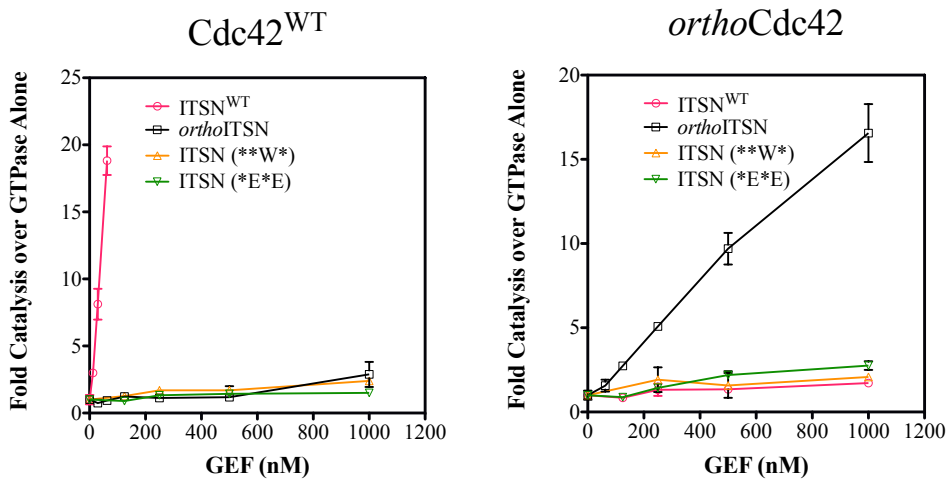


**Figure S3: Thermal denaturation by circular dichroism.**

Shown is the temperature dependence of the circular dichroism signal (mean residue ellipticity, MRE) at 222 nm for Cdc42 (left) and ITSN (right). Because thermal melts are irreversible for both proteins, the curves cannot be interpreted in terms of equilibrium denaturation, but indicate similar onset of melting for wild-type (pink symbols) and engineered variants (black symbols).

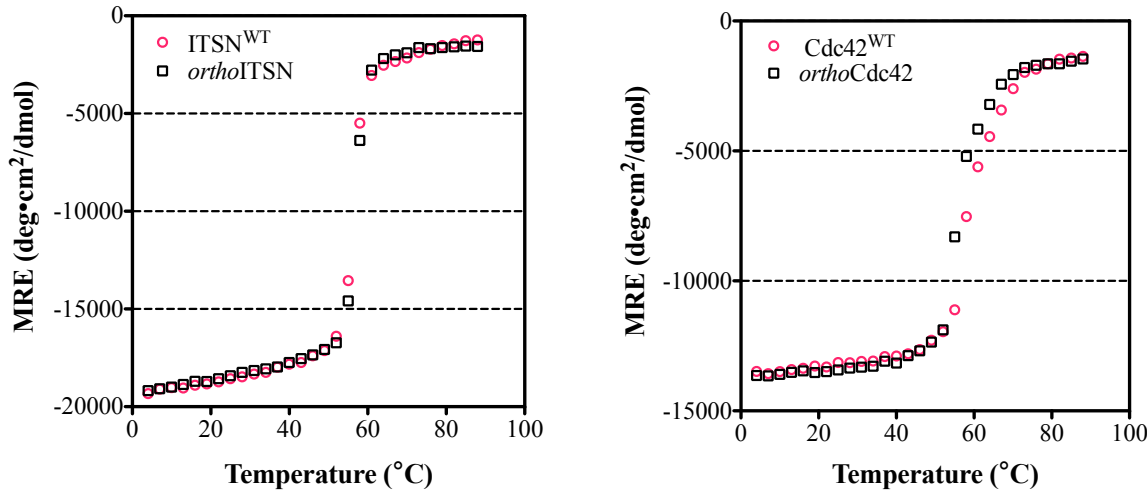


**Figure S4: Raw biacore sensorgram data.**

Shown are raw data from Cdc42<sup>WT</sup> (left) or *ortho*Cdc42 (right) flowing over a cell with immobilized ITSN<sup>WT</sup> (left: pink curves; right: grey curves) and a separate flow cell with immobilized *ortho*ITSN (left: grey curves; right: black curves) for different Cdc42 concentrations (10 nM to 5  $\mu$ M). Response units at saturation for each Cdc42 concentration were used to derive the equilibrium binding data shown in Figure 2C in the main manuscript. Curves for cognate pairs are pink (left) and black (right). Curves for non-cognate pairs are grey.

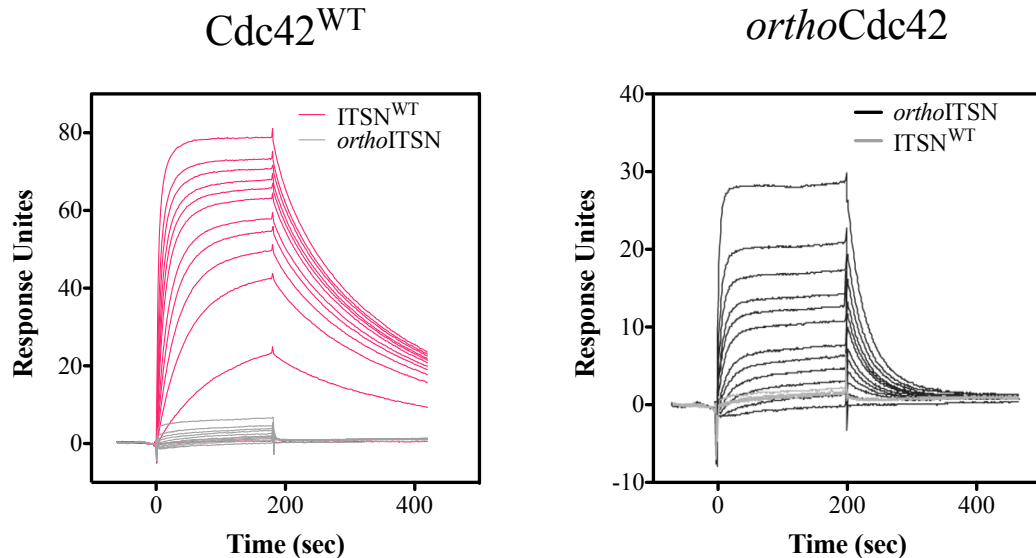


**Figure S5: Additional analysis of the structure of the designed *ortho*Cdc42/*ortho*ITSN complex.**

**(A)** The salt bridge interaction between the F56R and S1373E sidechains is revealed in a  $\sigma$ A-weighted simulated annealed composite omit electron density map calculated using the final model and contoured at  $1\sigma$ . ITSN in teal with green side chains, Cdc42 in gray with orange side chains, density contours in yellow.

**(B)** Details of side chain changes, comparing the Cdc42<sup>WT</sup>/ITSN<sup>WT</sup> complex (light gray with orange side chains / teal with light green side chains) to the engineered *ortho*Cdc42/*ortho*ITSN complex (dark gray with firebrick side chains / deep teal with dark green side chains). These changes involve reorganization of a polar interaction network and a flip of the Y40 side chain about the beta strand, which requires a rearrangement of M1369 as this residue occupies the position in the template structure that is taken by Y40 in the designed interface. The loop rearrangement also drastically changes the position of N39. Note that this view is in the same orientation as shown in **Fig. 3** in the main manuscript.

**(C)** Analysis of the GDP site in the designed *ortho*Cdc42/*ortho*ITSN complex (Green: *ortho*ITSN; dark grey: *ortho*Cdc42). The interface design mutations (S1373E, green; F56R, grey) are shown in stick representation with hydrogen bonds as dashed lines. GDP (yellow) is also shown in stick representation surrounded by electron density from a  $\sigma$ A-weighted kicked map contoured at  $1\sigma$ . The C $\beta$  atom of A59 is shown as a dark blue sphere and would clash with a Mg<sup>2+</sup> ion in the binding site.

**(D)** The binding site of the Cdc42<sup>WT</sup> structure (PDB ID: 1AN0, pink) is occupied by a GDP molecule (yellow sticks) and a Mg<sup>2+</sup> ion (represented as a small green sphere). The interface residue F56 is shown in sticks. The C $\beta$  atom of the A59 side chain is shown as a dark blue sphere and does not clash with the Mg<sup>2+</sup> ion.

**(E)** In the Cdc42<sup>WT</sup>/ITSN<sup>WT</sup> structure (PDB ID: 1KI1, cyan: ITSN<sup>WT</sup>; light grey; Cdc42<sup>WT</sup>), the C $\beta$  atom of A59 (shown as a dark blue sphere) would clash with a Mg<sup>2+</sup> ion in the binding site. The interface residues F56 and S1373 are shown in sticks. A sulfate ion (red spheres) is observed at a location that would occupy the position of the beta-phosphate of a GDP in the binding site. The presence of the SO<sub>4</sub><sup>2-</sup> ion suggests that even wild type Cdc42 can partially accommodate GDP-like ligands when bound to a GEF.

**Figure S5**

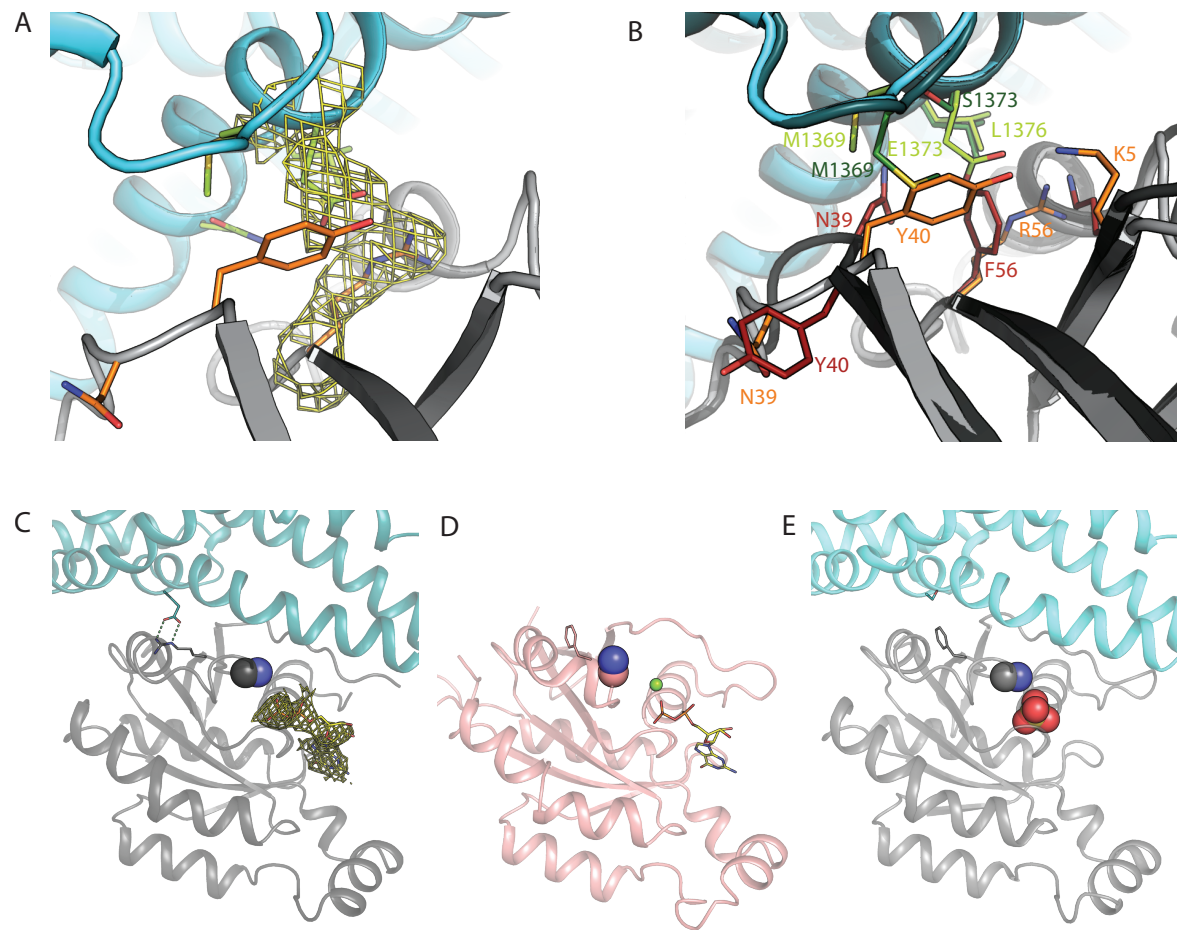


**Figure S6: Flexible backbone design and structure refinement strategy.**

(A) Flowchart of the general remodeling strategy implemented here, highlighting the alternating use of soft and hard repulsive forces, and indicating which panels provide details of simulation results for *ortho*Cdc42/*ortho*ITSN. Data in (B), (D) and (F) show the Rosetta full-atom energy versus the RMSD of the remodeled regions to the solved design structure. The RMSD between template and solved design structures is indicated by an orange line. (We note that the RMSD to the design structure was not used in selection of models or clustering). (B) Results of the initial backrub diversification simulations (step (2) in **SI Results**), with RMSDs that remain relatively close to that of the template. (C) Backrub ensemble of the template structure, from which the regions (red) sampled in the diversification simulations (step (3) in **SI Results**) were derived. Cdc42 in gray, ITSN in teal. (D) and (E) show the 10,000 decoys generated with soft repulsive KIC loop modeling on the selected flexible regions (step (3) in **SI Results**), with the RMSD to the solved structure in (D) and the RMSD to the template structure in (E). Panel (E) also highlights the decoys selected for further refinement (blue) following the log-scaling selection procedure described in **SI Results** step (4). (F) Results of hard repulsive vicinity KIC sampling (step (4) in **SI Results**), colored by the cluster each decoy was assigned to. Filled circles indicate that Y40 was in a similar conformation as observed in the crystal structure of the design (see panel G). Note that this conformation of the tyrosine side chain was only observed in cases with a low backbone RMSD with respect to the solved design structure. (G) Lowest-scoring members of each cluster (colors as in F, solved design structure in yellow), showing the position of the Y40 side chain. Cdc42 in gray, ITSN in teal.

**Figure S6**

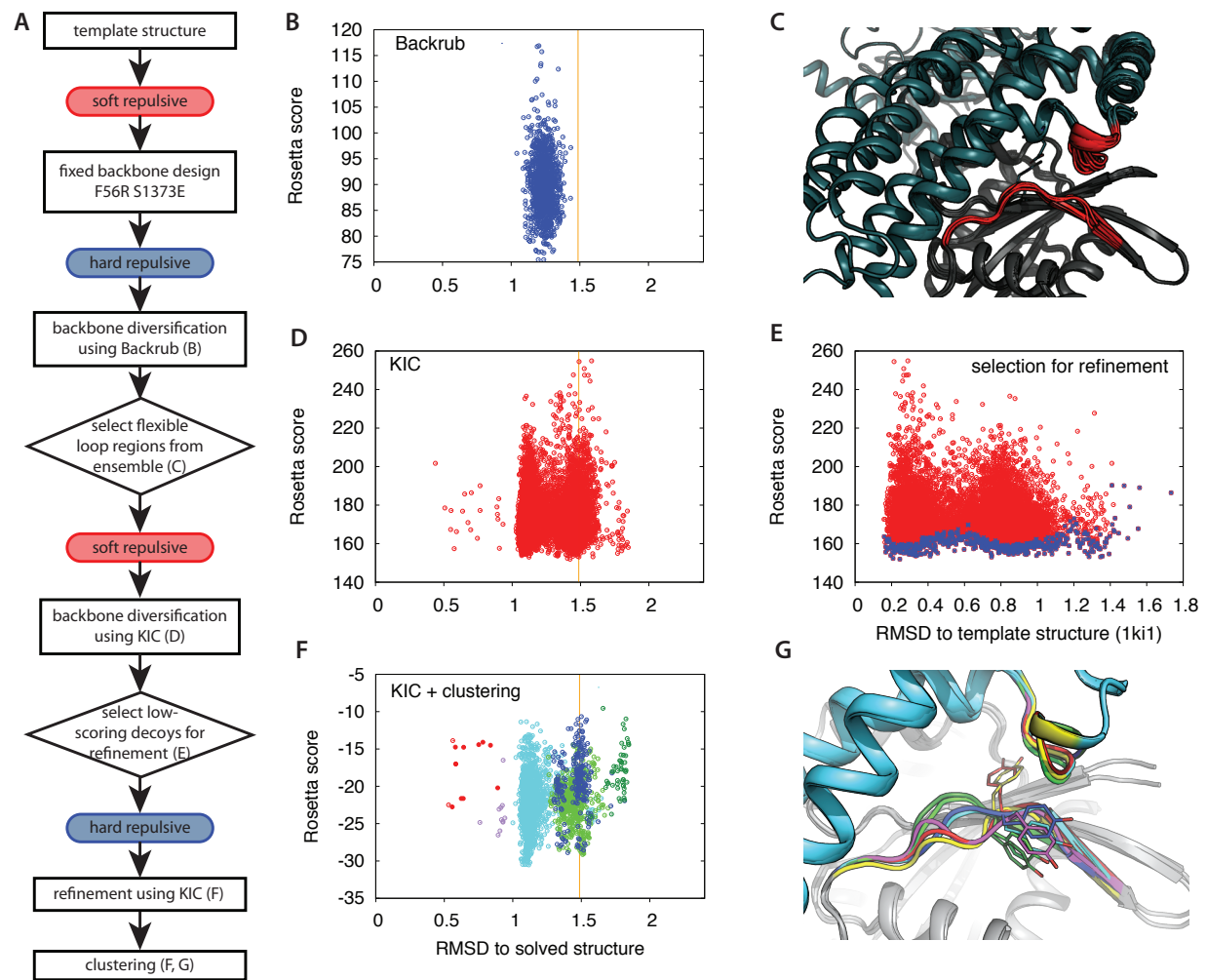


**Figure S7: Interaction of *ortho*Cdc42 with other GTPase circuit components.**

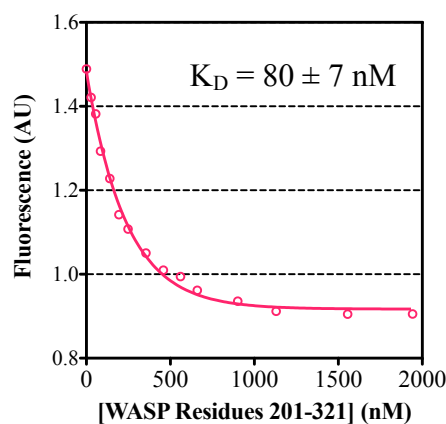
(A) Binding of WASP (residues 201-321) to Cdc42<sup>WT</sup> (left) and *ortho*Cdc42 (right) loaded with mant-GNPPNP, monitored by fluorescence quenching of mantGNPPNP by WASP.

(B) Rates of GTP hydrolysis of Cdc42 catalyzed by p50RhoGAP, as monitored by free phosphate release.

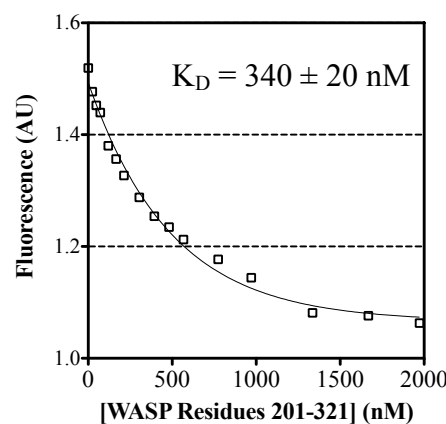
(C) Rho-GDI interaction. Cdc42 and RhoGDI form a stable complex and can be co-purified. Prenylated, His-tagged Cdc42 (the WT or F56R variant) were expressed in SF9 cells. GST-tagged RhoGDI was expressed in *E. coli*. SF9 and *E. coli* lysates were mixed and the Cdc42•RhoGDI complexes were purified using a Ni-NTA column followed by a GST-agarose column. Purified complexes were then run on an SDS-PAGE gel to verify that both the Cdc42 and RhoGDI proteins are present.

A

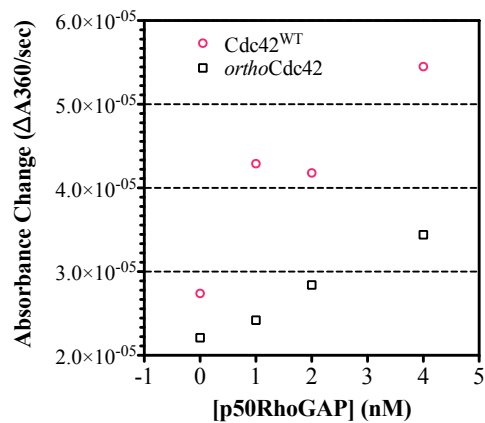
Cdc42<sup>WT</sup>



*ortho*Cdc42



B



C

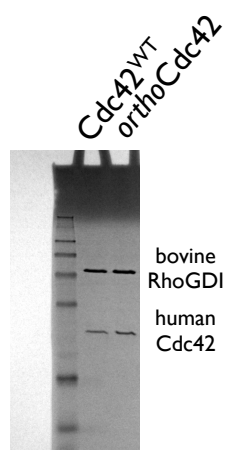


**Figure S8: Additional cell-based assays.**

(A) Time-course of Cdc42 activation after Rapamycin addition monitored by the G-LISA assay (**Methods**), as in **Figure 5B** in the main manuscript (**left**). Shown is the fold increase comparing samples with and without addition of Rapamycin at the indicated time. The total Cdc42 loaded in the G-LISA assay was determined by using an ELISA assay (**right**). Error bars represent the standard deviation of three experiments.

(B) Cell morphological changes monitored by the XCELLigence system (see **SI Methods** and **SI Results**). The normalized cell index reflects the measured change in impedance caused by changes in cell shape. Rapamycin was added at the 0-second time point. Error bars represent the standard deviation of three experiments.

(C) Cell retraction was observed as an additional phenotype under our experimental condition after the addition of Rapamycin.

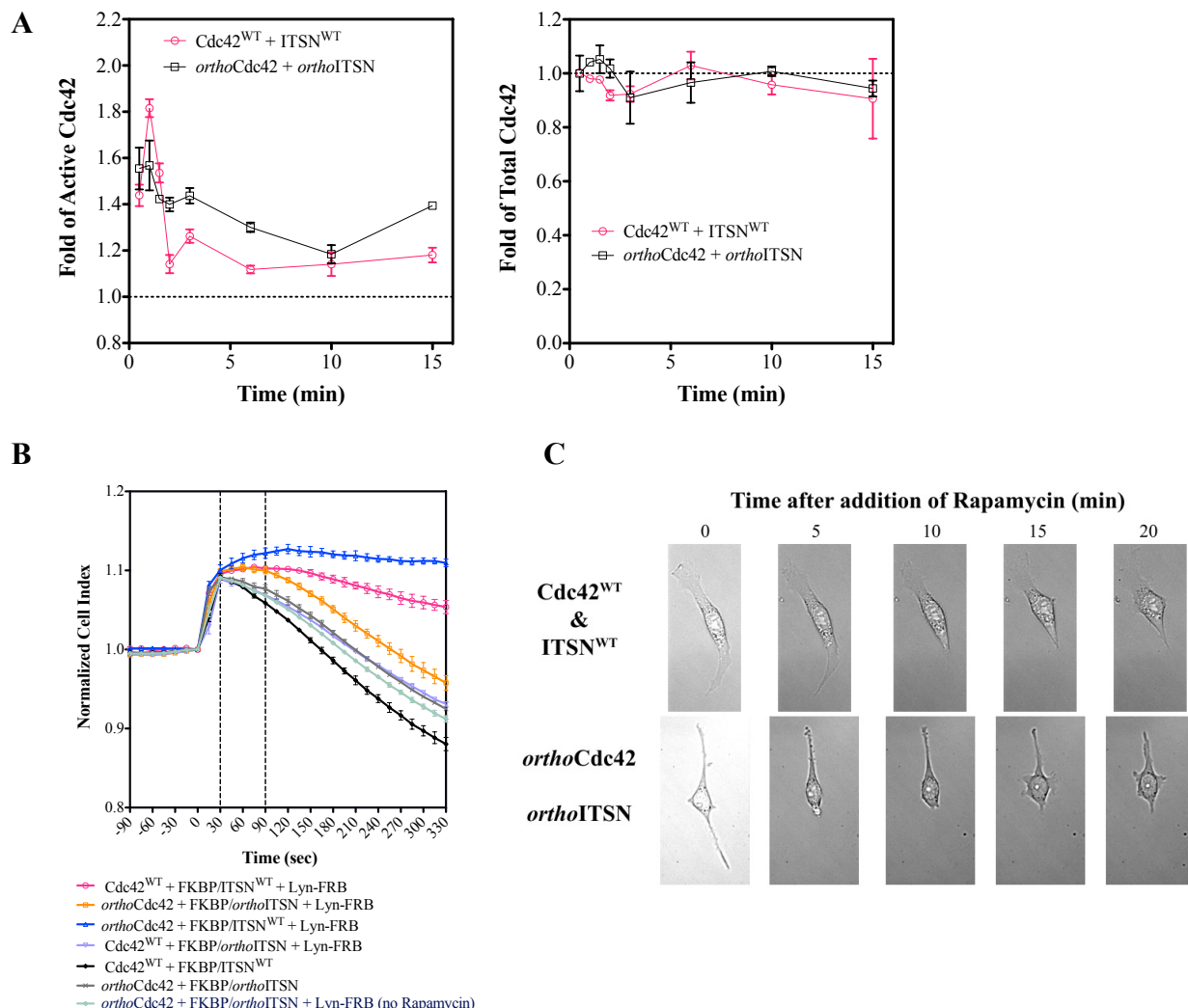


**Figure S9: Transferability of the designed R-E interaction to the Rac1/Tiam1 interface.**

Transferring the designed substitutions from *ortho*Cdc42/*ortho*ITSN to the equivalent positions in the Rac1-Tiam1 interface does not result in the same pattern of designed orthogonality. The left graph shows mantGDP dissociation from the GTPase Rac1<sup>WT</sup> in the absence of any exchange factor (gray open triangles) and in the presence of the wild-type exchange factor Tiam1<sup>WT</sup> (pink open circles) and the designed exchange factor Tiam1\* (S1184E, using PDB numbering from PDB ID 1FOE) (black open squares). The right graph shows dissociation from the designed GTPase Rac1\* (W56R) alone (grey open triangles) and in the presence of the same two exchange factor proteins.

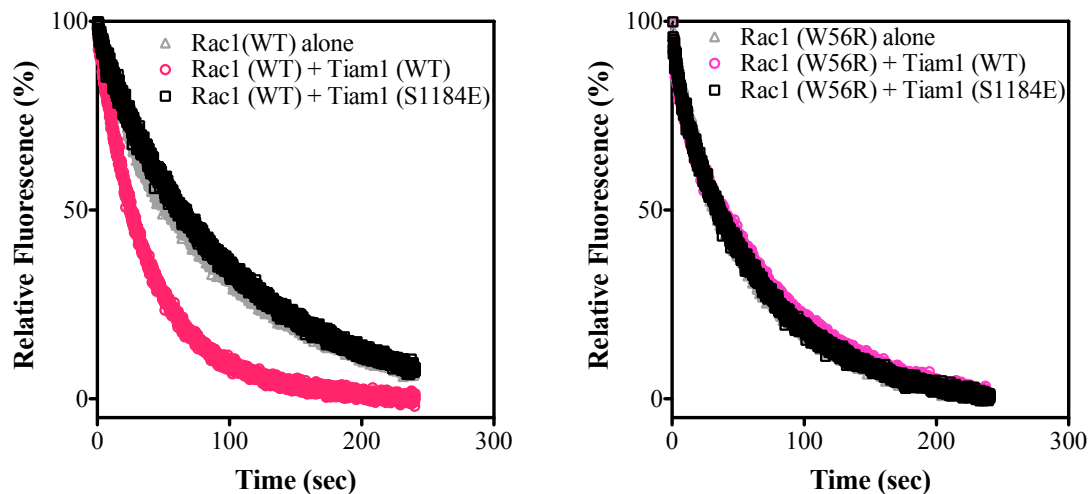
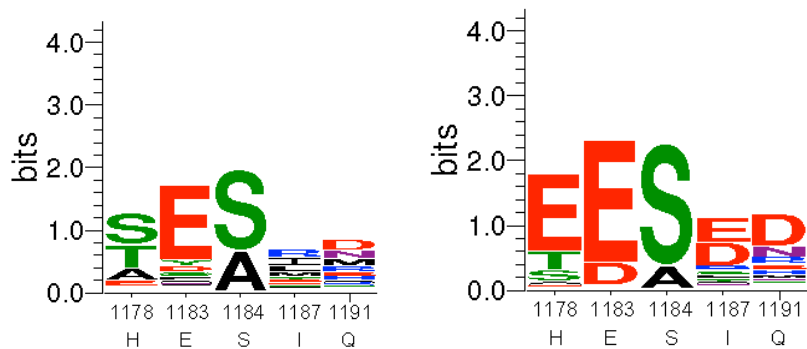


**Figure S10: Transferability of the designed R-E interaction to the Rac1/Tiam1 interface.**

Flexible backbone computational design predictions (**Methods**) for the five residues in Tiam1 (H1178, E1183, S1184, I1187 and Q1191) close to position 56 of Rac1 for Rac1<sup>WT</sup> (left) and Rac1\* (W56R) (right). Simulations are as shown in Figure 1D in the main manuscript, except that the backbone of the crystal structure of Rac1/Tiam1 (PDB ID: 1FOE (16)) was used as the starting conformation to create a backrub ensemble. Position S1184 is not enriched for glutamate.



## Supplementary Tables

**Table S1: Summary of designed Cdc42 and ITSN variants tested for orthogonality.**

Summary of the ability of different ITSN variant to catalyze nucleotide exchange in Cdc42<sup>WT</sup> or *ortho*Cdc42. Exchange activity was determined by mantGDP dissociation assays (<sup>a</sup>), mantGDP association assays (<sup>b</sup>), or both association and dissociation (<sup>c</sup>).

ITSN variant	Exchange activity with		Rationale
	Cdc42 <sup>WT</sup>	<i>ortho</i> Cdc42	
WT	+ <sup>c</sup>	- <sup>c</sup>	control
S1373E ( <i>ortho</i> ITSN)	- <sup>c</sup>	+ <sup>c</sup>	single substitution designed to form specific interaction with F56R in <i>ortho</i> Cdc42
M1369L, S1373E, L1376I	- <sup>a</sup>	+ <sup>a</sup>	additional substitutions predicted to be favorable at the <i>ortho</i> ITSN/ <i>ortho</i> Cdc42 site: M1369L: designed substitution (Fig. 1D) L1376I: substitution in ITSN homologs
S1373E, Q1380E	- <sup>b</sup>	- <sup>b</sup>	additional Q1380E substitution predicted (incorrectly) by the fixed backbone design protocol (Fig. 1D) to stabilize the interaction with F56R in <i>ortho</i> Cdc42
L1376W	- <sup>b</sup>	- <sup>b</sup>	substitution predicted (incorrectly) to stabilize the interaction of ITSN with Cdc42 <sup>WT</sup> (Fig. S1C)

**Table S2: Crystallographic data and refinement statistics for the structure of the designed *ortho*Cdc42/*ortho*ITSN interaction.**

<i>ortho</i> Cdc42/ <i>ortho</i> ITSN	
<b>Data collection</b>	
Resolution	50-2.65 (2.74-2.65)
Wavelength	1.115872
Space Group	P2 <sub>1</sub>
Cell angles	85.460 80.062 94.591
Cell edges	90.00 108.23 90.00
I/σ	20.0 (2.7)
R <sub>sym</sub>	6.9% (41.2%)
Completeness	99.6% (97%)
Redundancy	3.9 (3.7)
Observed reflections	139536 (12758)
Unique reflections	35386 (3394)
<b>Refinement</b>	
Resolution	46-2.65
Reflections	35295
Free reflections	3499
R <sub>work</sub>	24.1
R <sub>free</sub>	28.4
<b>Structure</b>	
Number of atoms:	7073
Protein	6897
Solvent	120
Ligand	56
Average B-factor:	54.6
Protein	54.5
Solvent	43.0
Ligand	79.7
RMS Bonds	0.006
RMS Angles	1.001
Residues with Favored Ramachandran Angles	96.0%
Residues with Outlier Ramachandran Angles	0.0

Values in parentheses are for the highest resolution shell.

**Table S3: Summary of interactions of *orthoCdc42* and *orthoITSN* with other GEFs and GTPases.**

Top table: summary of nucleotide exchange catalysis of a range of exchange factors for Cdc42<sup>WT</sup> and *orthoCdc42*. Bottom table: exchange activity of ITSN<sup>WT</sup> and *orthoITSN* for different GTPases. Exchange activity was determined by mantGDP dissociation (<sup>a</sup>) or both association and dissociation (<sup>b</sup>). Data for RhoG were obtained with the DH domain of ITSN<sup>WT</sup> and *orthoITSN* only (<sup>c</sup>); all other assays used the DH-PH domain construct for ITSN.

GEF	Cdc42 <sup>WT</sup>	<i>orthoCdc42</i>
ITSN <sup>WT</sup>	+ <sup>b</sup>	- <sup>b</sup>
<i>orthoITSN</i>	- <sup>b</sup>	+ <sup>b</sup>
PREX	+ <sup>a</sup>	+ <sup>a</sup>
Tiam1	- <sup>a</sup>	- <sup>a</sup>
TrioN	- <sup>a</sup>	- <sup>a</sup>
Dbs	+ <sup>a</sup>	- <sup>a</sup>

GTPase	ITSN <sup>WT</sup>	<i>orthoITSN</i>
Cdc42 <sup>WT</sup>	+ <sup>b</sup>	- <sup>b</sup>
<i>orthoCdc42</i>	- <sup>b</sup>	+ <sup>b</sup>
Rac1	- <sup>a</sup>	- <sup>a</sup>
RhoA	- <sup>a</sup>	- <sup>a</sup>
RhoG <sup>c</sup>	- <sup>a</sup>	- <sup>a</sup>

**Table S4: All constructs used in the *in vitro* and cell-based assay**

Protein	Residues	Mutation	Origin	Vector	Digestion Sites	Resistance	Host	Usage	Ref>Note
Lyn-FRB	NA	--	--	pC4RHE	--	Amp	NIH 3T3	Cell-based assays	(17)
ITSN (DH-PH)	1229-1580	--	Human	YF-Rac1	EcoRI, BglII (ITSN)/BamHI(vector)	Kan	NIH 3T3	Cell-based assays	(17)
ITSN (DH-PH)	1229-1580	S1373E	Human	YF-Rac1	EcoRI, BglII (ITSN)/BamHI(vector)	Kan	NIH 3T3	Cell-based assays	(17)
Cdc42	1-191	--	Human	pAmCyan1-C1	BamHI, EcoRI	Kan	NIH 3T3	Cell-based assays	This study
Cdc42	1-191	F56R	Human	pAmCyan1-C1	BamHI, EcoRI	Kan	NIH 3T3	Cell-based assays	This study
ITSN (DH-PH)	1229-1580	1373E, 1380E	Human	pBY601	--	Amp	<i>E. coli</i>	Expression	This study
ITSN (DH-PH)	1229-1580	1373E	Human	pBY601	--	Amp	<i>E. coli</i>	Expression	This study
ITSN (DH-PH)	1229-1580	1376W	Human	pBY601	--	Amp	<i>E. coli</i>	Expression	This study
ITSN (DH-PH)	1229-1580	--	Human	pSH200	--	Amp	<i>E. coli</i>	Expression	Lim Lab
Cdc42	1-179	F56R	Human	pBH4	--	Amp	<i>E. coli</i>	Expression	This study
Cdc42	1-179	--	Human	pBH4	--	Amp	<i>E. coli</i>	Expression	Lim Lab
RhoGDI	1-204	C79S	Bovine	pJT159-pGEX-KG-GDI	--	Amp	<i>E. coli</i>	Expression	(18)
WASP	201-321	--	Human	pGEX-2T	--	Amp	<i>E. coli</i>	Expression	(9)
p50RhoGAP	206-439	--	Human	pBY614	--	--	<i>E. coli</i>	Expression	Lim Lab
Cdc42	1-191	--	Human	pFastBac-B	BamH1	Amp	SF9	Expression	This study
Cdc42	1-191	F56R	Human	pFastBac-B	BamH1	Amp	SF9	Expression	This study
Rac1	1-177	F78S	Human	pSH200	--	Amp	<i>E. coli</i>	Expression	Lim Lab
Rac1	1-177	W56R, F78S	Human	pSH200	--	Amp	<i>E. coli</i>	Expression	This study
RhoA	1-190	--	Human	pAD15	--	Amp	<i>E. coli</i>	Expression	Lim Lab
RhoG	1-188	--	Murine	pAD18	--	Amp	<i>E. coli</i>	Expression	Lim Lab
Tiam1	1033-1406	--	Murine	pAD1	--	Amp	<i>E. coli</i>	Expression	Lim Lab
Tiam1	1033-1406	S1184E	Murine	pAD1	--	Amp	<i>E. coli</i>	Expression	This study
PREX	63-402	--	Human	--	--	--	<i>E. coli</i>	Expression	Lim Lab
Tim	1166-1527	--	Human	pAD24	--	Amp	<i>E. coli</i>	Expression	Lim Lab
TrioN	1284-1595	--	Human	pAD2	--	Amp	<i>E. coli</i>	Expression	Lim Lab
Dbs	623-967	--	Human	--	--	Amp	<i>E. coli</i>	Expression	(19)

Lyn-FRB and YF-Rac1 were gifts from the Meyer lab. pAmCyan-C1 was bought from Clontech. pFastBac-B was purchased from Invitrogen. The DNA for the WASP fragment was graciously provided by the Wittinghofer laboratory.

## Supplementary References

1. Kortemme T, *et al.* (2004) Computational redesign of protein-protein interaction specificity. *Nat Struct Mol Biol* 11(4):371-379.
2. Smith CA & Kortemme T (2010) Structure-based prediction of the peptide sequence space recognized by natural and synthetic PDZ domains. *J Mol Biol* 402(2):460-474.
3. Pace CN, Vajdos F, Fee L, Grimsley G, & Gray T (1995) How to measure and predict the molar absorption coefficient of a protein. *Protein Sci* 4(11):2411-2423.
4. Yeh BJ, Rutigliano RJ, Deb A, Bar-Sagi D, & Lim WA (2007) Rewiring cellular morphology pathways with synthetic guanine nucleotide exchange factors. *Nature* 447(7144):596-600.
5. Minor W, Cymborowski M, Otwinowski Z, & Chruszcz M (2006) HKL-3000: the integration of data reduction and structure solution--from diffraction images to an initial model in minutes. *Acta Crystallogr D Biol Crystallogr* 62(Pt 8):859-866.
6. Trapani S & Navaza J (2008) AMoRe: classical and modern. *Acta Crystallogr D Biol Crystallogr* 64(Pt 1):11-16.
7. Emsley P, Lohkamp B, Scott WG, & Cowtan K (2010) Features and development of Coot. *Acta Crystallogr D Biol Crystallogr* 66(Pt 4):486-501.
8. Adams PD, *et al.* (2010) PHENIX: a comprehensive Python-based system for macromolecular structure solution. *Acta Crystallogr D Biol Crystallogr* 66(Pt 2):213-221.
9. Rudolph MG, *et al.* (1998) The Cdc42/Rac interactive binding region motif of the Wiskott Aldrich syndrome protein (WASP) is necessary but not sufficient for tight binding to Cdc42 and structure formation. *J Biol Chem* 273(29):18067-18076.
10. Zhang B, Wang ZX, & Zheng Y (1997) Characterization of the interactions between the small GTPase Cdc42 and its GTPase-activating proteins and putative effectors. Comparison of kinetic properties of Cdc42 binding to the Cdc42-interactive domains. *J Biol Chem* 272(35):21999-22007.
11. Yu N, *et al.* (2006) Real-time monitoring of morphological changes in living cells by electronic cell sensor arrays: an approach to study G protein-coupled receptors. *Anal Chem* 78(1):35-43.
12. Qian B, *et al.* (2007) High-resolution structure prediction and the crystallographic phase problem. *Nature* 450(7167):259-264.
13. Smith CA & Kortemme T (2008) Backrub-like backbone simulation recapitulates natural protein conformational variability and improves mutant side-chain prediction. *J Mol Biol* 380(4):742-756.
14. Mandell DJ, Coutsias EA, & Kortemme T (2009) Sub-angstrom accuracy in protein loop reconstruction by robotics-inspired conformational sampling. *Nature methods* 6(8):551-552.
15. Khatib F, *et al.* (2011) Algorithm discovery by protein folding game players. *Proceedings of the National Academy of Sciences of the United States of America* 108(47):18949-18953.
16. Worthylake DK, Rossman KL, & Sondek J (2000) Crystal structure of Rac1 in complex with the guanine nucleotide exchange region of Tiam1. *Nature* 408(6813):682-688.
17. Inoue T, Heo WD, Grimley JS, Wandless TJ, & Meyer T (2005) An inducible translocation strategy to rapidly activate and inhibit small GTPase signaling pathways. *Nat Methods* 2(6):415-418.
18. Co C, Wong DT, Gierke S, Chang V, & Taunton J (2007) Mechanism of actin network attachment to moving membranes: barbed end capture by N-WASP WH2 domains. *Cell* 128(5):901-913.
19. Rossman KL, *et al.* (2002) A crystallographic view of interactions between Dbs and Cdc42: PH domain-assisted guanine nucleotide exchange. *EMBO J* 21(6):1315-1326.